

AN ANALYSIS OF THE STATIC AND DYNAMIC
CHARACTERISTICS OF A DECOUPLED LANDING ENTRY VEHICLE

By

James Ernest Haile

Thesis submitted to the Graduate Faculty of the

Virginia Polytechnic Institute

in candidacy for the degree of

MASTER OF SCIENCE

in

AEROSPACE ENGINEERING

May 1968

AN ANALYSIS OF THE STATIC AND DYNAMIC
CHARACTERISTICS OF A DECOUPLED LANDING ENTRY VEHICLE

By

James Ernest Haile

Thesis submitted to the Graduate Faculty of the
Virginia Polytechnic Institute
in candidacy for the degree of

MASTER OF SCIENCE

in

AEROSPACE ENGINEERING

APPROVED:

Chairman

F.H. Lutze
F.H. Lutze

W.D. Smith

F.R. DeJarnette

Date

May 1968

Blacksburg, Virginia

I. TABLE OF CONTENTS

CHAPTER	PAGE
I. TABLE OF CONTENTS	ii
II. ACKNOWLEDGEMENTS	iii
III. LIST OF FIGURES	iv
IV. INTRODUCTION	1
V. LIST OF SYMBOLS	4
VI. THEORETICAL ANALYSIS	8
Basic Body Description	8
Basic Body Aerodynamic Analysis	8
Handling Qualities	11
Derivation of $\frac{s_a}{s_d}$	11
Derivation of $\left \frac{s_a}{p_a} \right $	16
Static Stabilizing Devices	18
Entry Trajectory	20
Transient Response	21
Longitudinal	21
Lateral-Directional	22
VII. CONCLUDING REMARKS	23
VIII. REFERENCES	24
IX. APPENDIX	26
A. Table of Vehicle Characteristics Used in Dynamic Analysis	26
B. Derivation of Dynamic Stability Equations using Newtonian Impact Theory	28
X. FIGURES	30
XI. VITA	44

II. ACKNOWLEDGEMENTS

The author wishes to express his appreciation to the National Aeronautics and Space Administration for permission to use the material in this thesis, which was partially obtained from research projects at the Langley Research Center.

He also wishes to thank _____ and _____ of the Aerospace Engineering Department of the Virginia Polytechnic Institute, for their advice and assistance in preparing this thesis.

Finally, the author wishes to thank his wife who typed the text and provided encouragement throughout this period.

III. LIST OF FIGURES

FIGURE	PAGE
1. Basic body definition	30
2. Comparison of basic body theoretical and experimental aerodynamic characteristics	31
(a) Performance	31
(b) Body axis	32
(c) Lateral-directional static stability	33
3. Axis system	34
4. Definition of stability and control devices	
(a) Complete vehicle	35
(b) Componets	36
5. Vehicle trimmed aerodynamic characteristics	37
(a) Longitudinal stability	37
(b) Lateral-directional stability.	38
(c) Performance	39
6. Reentry vehicle handling qualities	40
7. Trajectory for a maximum performance entry	41
8. Longitudinal transient characteristics	42
9. Lateral-directional transient characteristics	43

IV INTRODUCTION

Several lifting entry vehicle studies at the Langley Research Center have dealt with the design of an entry vehicle with a high lift-to-drag ratio. However, to design such a vehicle, which will be stable in hypersonic, supersonic, and subsonic flight, generally requires conflicting design criteria. The stability and control devices required for subsonic and supersonic flight result in hypersonic performance penalties. These compromises in performance make the high L/D requirement difficult to satisfy.

A means to eliminate this aerodynamic conflict is to optimize the vehicle for the important hypersonic flight regime, with the understanding that the vehicle will be assisted through the supersonic flight regime by some auxiliary device. A vehicle employing this concept is called a "decoupled landing entry vehicle", due to the hypersonic aerodynamics being "decoupled" from the supersonic-subsonic aerodynamics (see reference 1). Employing the decoupled landing concept permits the consideration of simpler shapes which yield the highest level of performance in the hypersonic regime. The more prominent decoupled systems under study are the gliding parachute with impact-attenuation systems, limp paraglider, autorotative rotor, powered rotor, and sustained propulsive lift. A semi-decoupled device under consideration would utilize the subsonic aerodynamic characteristics of the vehicle by deploying stowed wings.

With the recent development of a hypersonic arbitrary-body aerodynamic computer program, it is possible to theoretically obtain a detailed hypersonic aerodynamic analysis of a complex body. In addition to computing the static characteristics of the body, the program will also compute the dynamic stability derivatives, using Newtonian impact theory. These static and dynamic stability derivatives, can then be used as inputs for an analysis of the dynamic characteristics of the vehicle. This enables a total analysis of a system in a preliminary design stage.

The purpose of this investigation is to define the static and dynamic characteristics of the Langley Research Center sponsored DL-4 (decoupled lander, number 4) entry vehicle. A Hypersonic arbitrary-body aerodynamic computer program is used to determine the aerodynamics of the basic body. Three theories are used and compared with data obtained for Mach number equal to nineteen. Several stabilizing devices are investigated to determine which are the most effective in providing static stability. To evaluate the lateral-directional handling qualities, a $\frac{\omega}{\omega_d} \frac{\phi}{\beta}$ coupling parameter, along with the $\left| \frac{\phi}{\beta} \right|$ parameter are derived to be applicable during hypersonic entry. Equations are also derived for determining the contribution of the stabilizing devices to the dynamic stability derivatives. In the evaluation of the vehicle dynamic characteristics, linearized equations of motion for the longitudinal and lateral-directional modes are used at several points along a maximum performance

trajectory. The parameters considered throughout the trajectory are the period and the time to damp to one-half amplitude.

V. LIST OF SYMBOLS

b	reference span, feet
C_A	axial-force coefficient, $\frac{\text{axial force}}{q_\infty S}$
C_D	drag coefficient, $\frac{\text{drag}}{q_\infty S}$
C_L	lift coefficient, $\frac{\text{lift}}{q_\infty S}$
C_l	rolling-moment coefficient, $\frac{L}{q_\infty S b}$
C_m	pitching-moment coefficient, $\frac{M}{q_\infty S b}$
C_N	normal-force coefficient, $\frac{\text{normal force}}{q_\infty S}$
C_n	yawing-moment coefficient, $\frac{N}{q_\infty S b}$
C_Y	side-force coefficient, $\frac{\text{side force}}{q_\infty S}$
g	acceleration due to gravity, feet/second ²
$\hat{i}, \hat{j}, \hat{k}$	unit vectors in x, y, z directions
i	imaginary number, $\sqrt{-1}$
I_x, I_y, I_z	principal moments of inertia, slug-feet ²
L	rolling moment, foot/pounds
L'	= $\frac{L}{I_x}$
L'_k	= $\frac{\partial L'}{\partial k}$; k = $\alpha, \beta, r,$ or δ_a
L/D	lift-drag ratio
l	reference length, feet
M	pitching moment, foot/pounds
m	vehicle mass, slugs
N	yawing moment, foot/pounds

N'	=	$\frac{N}{I_z}$
N'_k	=	$\frac{\partial N'}{\partial k}$; $k = r, \beta, p, \text{ or } \delta_a$
\hat{N}		unit surface normal (see Appendix B)
n_x, n_y, n_z		direction cosines of \hat{N}
C		order of magnitude
P		period, seconds
p		rolling angular velocity, radians/second
q		pitching angular velocity, radians/second
q_∞		free-stream dynamic pressure, $1/2 \rho_\infty v_\infty^2$, pounds/foot ²
r		yawing angular velocity, radians/second
S		body projected area, feet ²
s		Laplace operator
$t_{1/2}$		time to damp to one-half amplitude, seconds
V_∞		free-stream velocity, feet/second
\hat{V}_∞		unit free-stream velocity vector
\hat{V}_T		unit total velocity vector
W		weight, pounds
X_c, Y_c, Z_c		components of \bar{p} , feet
XYZ		body reference axis (see figure 3)
Y		side force, pounds
Y'	=	$\frac{Y}{mV_\infty}$
Y'_k		$\frac{\partial Y'}{\partial k}$; $k = p, r, \beta, \text{ or } \delta_a$
α		angle of attack, degrees

β	angle of side slip, degrees
γ	flight-path angle
δ_a	aileron deflection ($\delta_{eR} - \delta_{eL}$), degrees
δ_e	elevon deflection $\left(\frac{\delta_{eR} + \delta_{eL}}{2}\right)$, degrees
δ_{eR}	deflection of right elevon, positive with trailing edge down, degrees
δ_{eL}	deflection of left elevon, positive with trailing edge down, degrees
ΔA	elemental surface area, feet ²
$\Delta \bar{F}$	elemental force vector, pounds
$\Delta \bar{M}$	$= L\hat{i} + M\hat{j} + N\hat{k}$
ϵ	toe-in angle, degrees
ϕ	roll-out angle, degrees
\bar{p}	position vector (see Appendix B), feet
ρ_∞	free-stream air density, slugs/foot ³
T_R	roll time constant
θ	Newtonian angle (see Appendix B)
ω_d	undamped natural frequency of Dutch roll mode, radians/second
ω_p	undamped natural frequency of numerator quadratic in aileron to roll transfer function, radians/second
$\frac{\omega_p}{\omega_d}$	steady-state rolling effectiveness parameter
ζ_p	damping ratio of numerator quadratic in roll to aileron transfer function

ζ_d	=	Dutch roll damping ratio
C_{l_p}	=	$\frac{\partial C_l}{\partial \left(\frac{pb}{2V_\infty}\right)}$, per radian
C_{l_r}	=	$\frac{\partial C_l}{\partial \left(\frac{rb}{2V_\infty}\right)}$, per radian
C_{l_β}	=	$\frac{\partial C_l}{\partial \beta}$, per degree
$C_{l_{\delta_a}}$	=	$\frac{\partial C_l}{\partial \delta_a}$, per radian
C_{m_q}	=	$\frac{\partial C_m}{\partial \left(\frac{ql}{2V_\infty}\right)}$, per radian
C_{m_a}	=	$\frac{\partial C_m}{\partial a}$, per radian
$C_{m_{\delta_e}}$	=	$\frac{\partial C_m}{\partial \delta_e}$, per radian
C_{n_p}	=	$\frac{\partial C_n}{\partial \left(\frac{pb}{2V_\infty}\right)}$, per radian
C_{n_r}	=	$\frac{\partial C_n}{\partial \left(\frac{rb}{2V_\infty}\right)}$, per radian
C_{n_β}	=	$\frac{\partial C_n}{\partial \beta}$, per degree
$C_{n_{\delta_a}}$	=	$\frac{\partial C_n}{\partial \delta_a}$, per radian
C_{Y_β}	=	$\frac{\partial C_Y}{\partial \beta}$, per degree
(.)	=	$\frac{\partial (\quad)}{\partial t}$, per second

VI THEORETICAL ANALYSIS

Basic Body Description

Figure 1 shows a drawing of the basic body which was generated from a parabola of revolution. Cross sections of the parabola of revolution are indicated by the circles around the various cross sectional views in figure 1. The canopy was designed to accommodate one man with adequate landing visibility for a 38-foot long vehicle. Aft of the canopy the width is sufficient to accommodate two men side by side. The flat top is of sufficient width to accommodate stowed landing aids. In a preliminary layout of this vehicle it was determined that the center of gravity from weight and balance considerations would be at approximately 61 percent of the body length. From this layout the mass and inertias of a 38-foot length vehicle were determined and are listed in Appendix A.

Basic Body Aerodynamic Analysis

The theoretical inviscid aerodynamic characteristics of the basic body was determined by use of a hypersonic arbitrary-body aerodynamic computer program and high-speed digital computer (reference 2). The pressure distribution of the body was determined by computing a pressure coefficient at a point for a given surface inclination relative to the wind. Approximately 800 body coordinates were used as inputs to the program for the mathematical definition

of the body.

Newtonian, tangent cone, and oblique-shock aerodynamic theories were used with the computer program. In the shadowed regions (where the surface inclination relative to the wind is negative) a pressure coefficient equal to zero was assumed for all three theories. Unlike Newtonian theory, the tangent cone and oblique-shock theories are undefined for the higher of the surface inclination angles (reference 3). Above this shock detachment angle, a continuous pressure coefficient distribution was assumed up to the maximum pressure coefficient. Since only small portions of the body surface were in the "detached" region for this limited angle of attack study, the accuracy of this pressure coefficient distribution had little effect on the calculated aerodynamic characteristics.

The theoretical static coefficients of the basic body are compared in figure 2 with measurements obtained in the Langley Research Center 22 inch Helium Tunnel ($M=19.1$). Newtonian impact theory predicted C_N and C_L accurately for the majority of the angles-of-attack (see figures 2 (a) and (b)). In the low angle-of-attack range, however, complex flow patterns, possibly including flow separation, in the vicinity of the canopy, probably contributed to the difference between theoretical and experimental values of C_N and C_L . Since none of the theories account for skin friction contribution, the predictions for C_A were considerably

lower than experimental values throughout the angle-of-attack range.

Although the use of Newtonian theory resulted in good predictions of C_N and trends of C_A with angle of attack, apparently the longitudinal distributions of pressures and elemental normal forces were slightly in error. The theoretical C_m was somewhat below the measured values throughout most of the angle-of-attack range (figure 2 (b)); this difference represents an error in center of pressure location of no more than 4 percent of the body length. Likewise, the theoretical C_y differed somewhat from the measured values. It is of interest, however, that for the lateral-directional stability parameters (figure 2 (c)), the trends with angle-of-attack are predicted.

It may be concluded that, for this particular shaped vehicle, Newtonian impact theory gives good results for C_N and C_L . However, for all other static parameters, the trends may be predicted, but the magnitudes are somewhat in error. Consequently, in the consideration of stability and control devices, the measured body aerodynamic characteristics will be used as the reference characteristics. Newtonian impact theory will be used to predict the aerodynamic characteristics of the stability and control devices. It is assumed that this combination of basic body data plus Newtonian impact theory increments will give a good approximation of the vehicle aerodynamic characteristics.

Handling Qualities Criteria

Investigations have shown that for an aircraft to have acceptable handling qualities, the lateral-directional response to an aileron control input must satisfy certain criteria (reference 4). This criteria has been defined from recent simulator studies for an entry vehicle (reference 5). In reference 5, pilot opinion was correlated to a $\frac{\omega}{\omega_d}$ coupling parameter and $\left|\frac{\phi}{\beta}\right|$. In general, it was concluded that pilot opinion was optimum when the general three degree of freedom response to an aileron input was reduced to a single degree response in roll, with no Dutch roll excitation. To use this criteria for hypersonic vehicle design, it is necessary to derive the $\frac{\omega}{\omega_d}$ and $\left|\frac{\phi}{\beta}\right|$ parameters.

Derivation of $\frac{\omega}{\omega_d}$.- The lateral-directional equations of motion

for a vehicle with a body-fixed axis system (figure 3) and x-z plane of symmetry are given below (see reference 6):

$$\left. \begin{aligned} L &= I_x \dot{p} - I_{xz} \dot{r} + qr(I_z - I_y) - I_{xz} pq \\ N &= -I_{xz} \dot{p} + I_z \dot{r} + pq(I_y - I_x) + I_{xz} qr \\ Y + mg \cos \delta \sin \eta &= m(\dot{V} + rU + \dot{w}) \end{aligned} \right\} (1)$$

where

$$\bar{V}_\infty = V\hat{i} + U\hat{j} + W\hat{k}$$

To simplify the above equations, appropriate approximations will be made. The assumptions that are necessary for simplification are:

1. The products qr and pq are small with respect to other terms.
2. The body axis coincides with the principal axis.

Using assumptions 1 and 2, equation set (1) reduces to:

$$\begin{aligned}
 L &= I_x \dot{\beta} \\
 N &= I_z \dot{\beta} \\
 Y + mg \cos \delta \sin \phi &= m(\dot{V} + rU + \dot{w})
 \end{aligned}
 \quad \left. \vphantom{\begin{aligned} L &= I_x \dot{\beta} \\ N &= I_z \dot{\beta} \\ Y + mg \cos \delta \sin \phi &= m(\dot{V} + rU + \dot{w}) \end{aligned}} \right\} (2)$$

For a body-fixed axis system, the free stream velocity components may be defined in the following manner:

$$\begin{aligned}
 \bar{V}_\infty &= U\hat{i} + V\hat{j} + W\hat{k} \\
 U &= V_\infty \cos \beta \cos \alpha \\
 V &= V_\infty \sin \beta \\
 W &= V_\infty \cos \beta \sin \alpha
 \end{aligned}
 \quad \left. \vphantom{\begin{aligned} \bar{V}_\infty &= U\hat{i} + V\hat{j} + W\hat{k} \\ U &= V_\infty \cos \beta \cos \alpha \\ V &= V_\infty \sin \beta \\ W &= V_\infty \cos \beta \sin \alpha \end{aligned}} \right\} (3)$$

Assumption 3: α is constant and β is small, such that

$$\sin \beta \approx \beta \text{ and } \cos \beta \approx 1$$

With assumption 3, equation set (3) reduces to

$$\begin{aligned}
 U &= V_\infty \cos \alpha \\
 V &= V_\infty \beta \\
 W &= V_\infty \sin \alpha
 \end{aligned}
 \quad \left. \vphantom{\begin{aligned} U &= V_\infty \cos \alpha \\ V &= V_\infty \beta \\ W &= V_\infty \sin \alpha \end{aligned}} \right\} (4)$$

Assumption 4: All stability derivatives are linear.

Assumption 5: L_r , L_β , N_β , N_r , Y_β , Y_r , and Y_β stability derivatives are negligible with respect to the other stability derivatives.

Using assumption 4 and 5, and equation set (4), equation set (2) becomes

$$\begin{aligned}
 L_\beta \dot{\beta} + L_\beta \beta + L_{\delta \alpha} \delta \alpha &= I_x \dot{\beta} \\
 N_r \dot{\beta} + N_\beta \beta + N_{\delta \alpha} \delta \alpha &= I_z \dot{\beta} \\
 Y_\beta \dot{\beta} + mg \cos \delta \sin \phi &= mV_\infty (\dot{\beta} + r \cos \alpha - \dot{w} \sin \alpha)
 \end{aligned}
 \quad \left. \vphantom{\begin{aligned} L_\beta \dot{\beta} + L_\beta \beta + L_{\delta \alpha} \delta \alpha &= I_x \dot{\beta} \\ N_r \dot{\beta} + N_\beta \beta + N_{\delta \alpha} \delta \alpha &= I_z \dot{\beta} \\ Y_\beta \dot{\beta} + mg \cos \delta \sin \phi &= mV_\infty (\dot{\beta} + r \cos \alpha - \dot{w} \sin \alpha) \end{aligned}} \right\} (5)$$

Assumption 6: The bank angle is restricted to small values, such that $|Y_\beta \beta| \gg |mg \cos \delta \sin \phi|$.

The following are defined:

$$\left. \begin{aligned} \frac{L}{I_x} &= L' \\ \frac{N}{I_z} &= N' \\ \frac{Y}{mV_\infty} &= Y' \end{aligned} \right\} (6)$$

Using equation set (6) and assumption (6), equation set (5) reduces to

$$\left. \begin{aligned} L'_p \dot{p} + L'_f \dot{f} + L'_{\delta a} \delta a &= \dot{p} \\ N'_r \dot{r} + N'_f \dot{f} + N'_{\delta a} \delta a &= \dot{r} \\ Y'_f \dot{f} &= \dot{\beta} + r \cos \alpha - p \sin \alpha \end{aligned} \right\} (7)$$

Rearranging equation set (7)

$$\left. \begin{aligned} L'_f \dot{f} + (L'_p \dot{p} - \dot{p}) &= -L'_{\delta a} \delta a \\ N'_f \dot{f} + (N'_r \dot{r} - \dot{r}) &= -N'_{\delta a} \delta a \\ (Y'_f \dot{f} - \dot{\beta}) + p \sin \alpha - r \cos \alpha &= 0 \end{aligned} \right\} (8)$$

Assumption 7: All initial conditions are zero.

Taking the Laplace transform of equation set (8) and applying assumption 7, equation set (8) becomes:

$$\left. \begin{aligned} L'_f \bar{f} + (L'_p - s) \bar{p} &= -L'_{\delta a} \delta a \\ N'_f \bar{f} + (N'_r - s) \bar{r} &= -N'_{\delta a} \delta a \\ (Y'_f \bar{f} - s) \bar{f} + \bar{p} \sin \alpha - \bar{r} \cos \alpha &= 0 \end{aligned} \right\} (9)$$

Or, in matrix form:

$$\begin{bmatrix} L'_f & (L'_p - s) & 0 \\ N'_f & 0 & (N'_r - s) \\ (Y'_f - s) & \sin \alpha & -\cos \alpha \end{bmatrix} \begin{Bmatrix} \bar{f} \\ \bar{p} \\ \bar{r} \end{Bmatrix} = \begin{Bmatrix} -L'_{\delta a} \delta a \\ -N'_{\delta a} \delta a \\ C \end{Bmatrix} \quad (10)$$

Premultiplying equation (10) with the inverse of the square matrix, equation (10) becomes:

$$\begin{bmatrix} \bar{p} \\ \bar{q} \\ \bar{r} \end{bmatrix} = \frac{1}{\Delta} \begin{bmatrix} -(N'_r - s)\sin\alpha & (L'_p - s)\cos\alpha & \\ (N'_p \cos\alpha + (N'_r - s)(Y'_f - s)) & -L'_f \cos\alpha & \\ N'_f \sin\alpha & ((L'_p - s)(Y'_f - s) - L'_c \sin\alpha) & \end{bmatrix} \begin{bmatrix} -L'_{\delta a} \bar{\delta a} \\ -N'_{\delta a} \bar{\delta a} \\ C \end{bmatrix} \quad (11)$$

Where,

$$\Delta = -s^3 + (L'_p + N'_r + Y'_f)s^2 + (L'_f \sin\alpha - L'_p N'_r - N'_f \cos\alpha - L'_p Y'_f - N'_r Y'_f)s + N'_f L'_p \cos\alpha + N'_r Y'_f L'_p - L'_f N'_r \sin\alpha$$

The desired transfer function is the roll rate to aileron deflection.

Expanding the second equation of (11) and rearranging terms, we obtain

$$\frac{\bar{p}}{\bar{\delta a}} = \frac{L'_{\delta a} (s^2 - (N'_r + Y'_f)s - L'_{\delta a} \frac{N'_{\delta a}}{L'_{\delta a}} \cos\alpha + N'_f \cos\alpha + N'_r Y'_f)}{-\Delta} \quad (12)$$

The general form of equation (12) may be expressed as:

$$\frac{\bar{p}}{\bar{\delta a}} = \frac{A_\omega (s^2 + 2\zeta_\omega \omega_\omega s + \omega_\omega^2)}{(s + 1/T_R)(s^2 + 2\zeta_d \omega_d s + \omega_d^2)} \quad (13)$$

To eliminate any Dutch roll response due to aileron input, the Dutch roll poles must be canceled by the numerator zeros. The conditions for this to occur require that

$$2\zeta_{\varphi}\omega_{\varphi} = 2\zeta_d\omega_d$$

$$\omega_{\varphi}^2 = \omega_d^2$$

An explicit function of $2\zeta_d\omega_d$ and ω_d^2 can not be determined from equation (12). However, the equation may be simplified by use of appropriate approximations.

Assumption 8: $|L_f^i|, |N_f^i| \gg |Y_f^i|, |L_o^i|, |N_r^i|$

Assumption 8 may be justified from the following orders of magnitude, which were determined from the values in Appendix A for conditions of $V_{\infty} = 10^4$ feet per second and an altitude of 125,000 feet.

$$\left. \begin{aligned} |L_f^i| &\rightarrow c(1) \\ |N_f^i| &\rightarrow c(1) \\ |Y_f^i| &\rightarrow c(10^{-3}) \\ |L_o^i| &\rightarrow c(10^{-4}) \\ |N_r^i| &\rightarrow c(10^{-4}) \end{aligned} \right\} (14)$$

Using the approximations of Assumption 8, equation (12) reduces to:

$$\frac{\bar{p}}{\delta a} = \frac{L_{\delta a}^i (s^2 + (-L_f^i \frac{N_{\delta a}^i}{L_{\delta a}^i} \cos \alpha + N_f^i \cos \alpha))}{s(s^2 + (-L_f^i \sin \alpha + N_f^i \cos \alpha))} \quad (15)$$

Therefore,

$$2\zeta_{\varphi}\omega_{\varphi} = 2\zeta_d\omega_d = 0$$

$$\omega_{\varphi}^2 = N_f^i \cos \alpha - L_f^i \frac{N_{\delta a}^i}{L_{\delta a}^i} \cos \alpha$$

$$\omega_d^2 = N_f^i \cos \alpha - L_f^i \sin \alpha$$

The coupling parameter then becomes:

$$\frac{\omega_p^2}{\omega_d^2} = \frac{N_f' \cos \alpha - L_f' \frac{N_{\delta a}'}{L_{\delta a}'} \cos \alpha}{N_f' \cos \alpha - L_f' \sin \alpha}$$

Rearranging and using non-dimensional stability derivatives:

$$\frac{\omega_p^2}{\omega_d^2} = \frac{1 - \frac{C_{l_f'} C_{n_{\delta a}'}}{C_{n_f'} C_{l_{\delta a}'}}}{1 - \frac{C_{l_f'} I_z \tan \alpha}{C_{n_f'} I_x}} \quad (16)$$

Equation (16) represents the desired result.

Derivation of $\left| \frac{\bar{p}}{\bar{r}} \right|$. - In reference 7, $\left| \frac{\bar{p}}{\bar{r}} \right|$ is defined as the ratio of Dutch-roll component in \bar{p} to the one in \bar{r} , in any particular transient response. The ratio is independent of the forcing function or initial conditions. It may be evaluated by setting the forcing functions of equation (9) to zero and dividing by \bar{r} . This yields the following:

$$\left. \begin{aligned} (L_f' - s) \frac{\bar{p}}{\bar{r}} &= -L_f' \\ (N_f' - s) \frac{\bar{p}}{\bar{r}} &= -N_f' \\ \frac{\bar{p}}{\bar{r}} \sin \alpha - \frac{\bar{r}}{\bar{r}} \cos \alpha &= -(Y_f' - s) \end{aligned} \right\} (17)$$

There are three possible combinations of equation (17) which will yield the same final solution to $\left| \frac{\bar{p}}{\bar{r}} \right|$. Choosing the first equation in (17) and rearranging we obtain

$$\frac{\bar{p}}{\bar{r}} = \frac{-L_f'}{(L_f' - s)}$$

or,

$$\frac{\bar{\varphi}}{\bar{f}} = \frac{-L_f'}{sL_n' - s^2} \quad (18)$$

Now, one of the Dutch roll roots must be substituted for s . Choosing

$$s = -\zeta_d \omega_d + i\omega_d \sqrt{1 - \zeta_d^2} \quad (19)$$

From equation (15) it was found that

$$\zeta_d \omega_d = 0 \quad (20)$$

$$\omega_d^2 = N_f' \cos \alpha - L_f' \sin \alpha$$

Equation (19) then becomes

$$s = i(N_f' \cos \alpha - L_f' \sin \alpha)^{1/2} \quad (21)$$

Substituting equation (21) into (18) we obtain

$$\frac{\bar{\varphi}}{\bar{f}} = \frac{-L_f'}{i(N_f' \cos \alpha - L_f' \sin \alpha)^{1/2} L_n' + (N_f' \cos \alpha - L_f' \sin \alpha)} \quad (22)$$

Using assumption 8, equation (22) reduces to

$$\left| \frac{\bar{\varphi}}{\bar{f}} \right| = \left| \frac{L_f'}{N_f' \cos \alpha - L_f' \sin \alpha} \right| \quad (23)$$

Expressing equation (24) in non-dimensional form:

$$\left| \frac{\bar{\varphi}}{\bar{f}} \right| = \left| \frac{1}{\frac{C_{n_f} I_x}{C_{l_f} I_z} \cos \alpha - \sin \alpha} \right| \quad (24)$$

Equation (24) represents the desired result.

Static Stabilizing Devices

In order to make the three static moments of the basic body stable, combinations of flat plates were added in the form of tip fins, elevons, fillets, and extensions. Newtonian impact theory was used to predict the aerodynamic contribution from these elements. The tip fins were analyzed by the equations presented in reference 8. To determine the dynamic stability derivatives of these devices, the necessary equations were derived in Appendix B. In the evaluation of lateral-directional handling qualities, equations 16 and 24 were used with data from reference 5.

To provide longitudinal and lateral control, trailing elevons were evaluated. Differential deflection of the two elevons provides roll control. In order to control yaw due to roll control deflection, the hinge lines were canted and a triangular aft extension included for elevon attachment. Several devices for providing directional and lateral stability were evaluated: dorsal fins, tip fins, combinations of dorsal and tip fins, and fillet plus tip fins. From this study it was determined that no combination of these stabilizing devices would satisfy the handling qualities criteria throughout the angle-of-attack range. The lateral-directional stability was therefore optimized at the maximum lift to drag condition, with the understanding that at other angles-of-attack some stability augmentation would be required.

From the results of calculations of various sizes and orientations of the tip fins, it was determined that a vertical tip fin toed-in 10° provided the best stability and control at $(L/D)_{\max}$, with a minimum loss in performance. Details of this fin are shown in figure 4. To fare the fin to the body, side extensions between the inner fin surface and bottom and side body surface were necessary. As shown in figure 4 the fins were trapezoidal with a 4° wedge section. The blended fin-body consisted of this tip fin blended to the body by use of the fin-body fillet (figure 4). The purpose of this fillet, in addition to providing attachment of the fin to the body, was to provide a positive pitching moment at zero lift.

The aerodynamics of the vehicle utilizing the above stabilizing devices is shown in figures 5 and 6. In figure 5 (a) it can be seen that the combination of fillet plus tip fins and elevons provide good trim capability. From the lateral-directional handling qualities criteria, it is necessary to have relatively large magnitudes of $C_{n\beta}$ and small magnitudes of $C_{l\beta}$. At $(L/D)_{\max}$ ($\alpha=10^\circ$) figure 5 (b) shows the relative magnitudes of the stability derivatives which provide optimum handling qualities. Figure 5 (c) shows that a 7.5 percent loss in $(L/D)_{\max}$ must be accepted by using these stability devices. Figure 6 presents the variation in the lateral directional handling qualities with changes in angle-of-attack. This parameter has not been considered in design of

previous entry vehicles. Because of the unconventionally high ratio in yaw to roll inertia ratio (14.3) the handling qualities are extremely sensitive to the magnitude of $C_{l\beta}$. For this vehicle good handling qualities can be attained at $\alpha=10^\circ$, but augmentation of $C_{l\beta}$ will be required for other operational angles-of-attack.

Entry Trajectory

For the evaluation of the dynamic characteristics of the vehicle, a maximum performance trajectory was used. Throughout entry, the angle-of-attack was held constant at the condition of maximum lift to drag ratio. Although this trajectory represents the maximum range condition, a pilot has the capability of varying his range through a bank angle modulation. This is the same concept used to provide Apollo with a variable range capability.

Using the conditions of maximum lift to drag in Appendix A, a constant angle of attack trajectory was calculated from an existing computer program at Langley Research Center. The computations were started at 400,000 feet altitude and an initial flight path angle of -1° . At 100,000 ft. altitude the computations were stopped, because the vehicle had decelerated into the supersonic flight regime. A plot of this trajectory is given in figure 7.

Transient Response

As mentioned previously, below 100,000 feet altitude the free stream velocity becomes supersonic. Above 200,000 feet, the dynamic

pressure and density are approaching free space conditions. Therefore, the operational range for investigation was selected to be between 100,000 and 200,000 feet altitude. To evaluate the transient response of the vehicle entering on a maximum performance trajectory, five points along the trajectory were selected and are shown in figure 7. At these five points the free stream density was computed using reference 9.

The transient characteristics of the vehicle were evaluated using linearized equations of motion similar to those of reference 6. The parameters of interest were the period and the time to damp to one-half amplitude. All of the vehicle characteristics used are listed in Table I.

Longitudinal.- In figure 8 are presented the characteristics of the short period mode. It indicates that above 100,000 feet altitude the transient motion is relatively slow with essentially no damping. It was found that the Phugoid mode is essentially negligible. Reference 10 indicates that a pilot should not encounter longitudinal controllability problems with this system provided the displacements and angular velocities are kept relatively small.

Lateral-directional.- In figure 9 the characteristics of the lateral-directional modes are presented. As with short period mode, the Dutch roll transient motion is relatively slow and essentially undamped. With the two aperiodic roll and spiral modes, the time to damp to one-half amplitude is of sufficient magnitude,

that for practical purposes they are negligible. Reference 5 indicates that with the existing satisfactory handling qualities, this configuration should pose no lateral-directional controlability problem.

VII CONCLUDING REMARKS

A theoretical analysis of the static and dynamic characteristics of an entry vehicle utilizing the decoupled landing concept has been conducted. This analysis has shown that a hypersonic arbitrary-body aerodynamic computer program can be used with Newtonian impact theory, for this class of vehicle, to predict the normal and lift forces with good accuracy, but the other forces and moments may be somewhat in error. In the analysis of the static stability devices, a set of tip fins plus fillet was found that provided stability with good handling qualities at the maximum performance angle-of-attack. However, deviations from this angle-of-attack condition cause the handling qualities to deteriorate to such an extent that a body alteration or augmentation of $C_{l\beta}$ will be required. The analysis of the transient response showed that the periodic modes were essentially undamped with long periods above 100,000 feet altitude. However, these transient characteristics should not pose a controllability problem to a pilot during a limited maneuvering entry.

VIII REFERENCES.

1. Love, Eugene S.: Manned Lifting Entry. *Astronautics and Aeronautics*, May 1966, pp. 54-64.
2. Gellert, George O.: Geometric Computing - Electronic Geometry for Semi-automatic Design. *Machine Design*, March 18, 1965, pp. 152-159.
3. Henderson, Authur; and Braswell, Dorothy: Charts for Conical and Two-Dimensional Oblique - Shock Flow Parameters in Helium at Mach Numbers from about 1 to 100. NASA TN D - 819, 1961.
4. Ashkeanas, I.L.; and McRuer, D.T.: The Determination of Lateral Handling Qualities Requirements from Airframe-Human Pilot Studies. WADC TR 59-135, June 1959.
5. Van Leynseele, Frank J.: Evaluation of Lateral-Directional Handling Qualities of Piloted Reentry Vehicles Utilizing a Fixed-Base Simulator. Proposed NASA TN, April, 1967.
6. Etkin, Bernard: *Dynamics of Flight*. John Wiley and Sons, Inc. New York, 1965.
7. Seckel, Edward: *Stability and Control of Airplanes and Helicopters*. Academic Press Inc., New York, 1964, p. 290.
8. Rainey, Robert W.; Haile, James E.; and Fenland, Jim A.: Prediction of Newtonian Aerodynamics of Bodies of Revolution and Toed-In-Rolled-Out Surfaces. NASA LWP - 549, 1968.

9. U.S. Standard Atmosphere, 1962. U.S. Government Printing Office, Washington 25, D.C., 1962.
10. Taylor, Laurence W.; and Day, Richard E.: Flight Controllability Limits and Related Human Transfer Functions as Determined from Simulator and Flight Tests. NASA TN D-746, 1961.

IX. APPENDIX

A. Table of Vehicle Characteristics
Used in Dynamic Analysis

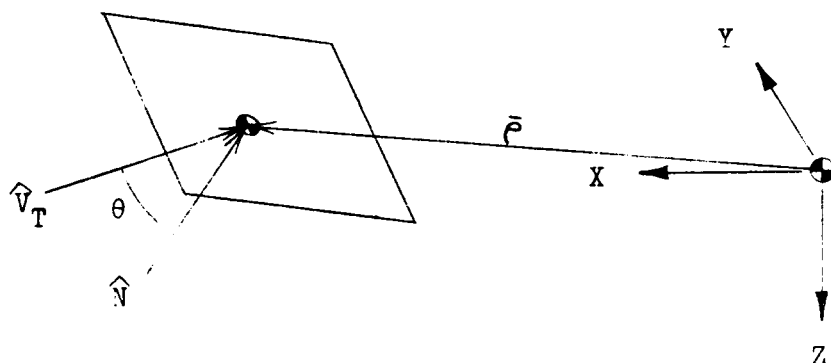
l	38 ft.
b	10.1 ft.
S	227 ft.
W	15,960 lb.
I_x	3500 slug-ft. ²
I_y	50,000 slug-ft. ²
I_z	50,000 slug-ft. ²
I_{xz}	0
a	10°
C_L	0.112
C_D	0.041
$C_{L\alpha}$	0.89 per radian
$C_{D\alpha}$	0.30 per radian
$C_{m\alpha}$	-0.0201 per radian
C_{mq}	-0.071 per radian
$C_{l\beta}$	-0.000007 per degree
$C_{n\beta}$	0.00098 per degree
$C_{y\beta}$	-0.0071 per degree
C_{lp}	-0.0166 per radian

C_{n_s}	-0.00048 per radian
C_{l_r}	-0.00048 per radian
C_{n_r}	-0.066 per radian
$C_{n_{\delta a}}$	0
$C_{l_{\delta a}}$	-0.0161 per radian

B.- Derivation of Dynamic Stability Derivative

Equations Using Newtonian Impact Theory

A flat surface is defined in the following manner:



The forces and moments of the flat plate, in the above figure, are defined as:

$$\Delta \bar{F} = C_p q_\infty \Delta A \hat{N} \quad (1)$$

$$\Delta \bar{M} = C_D q_\infty \Delta A (\bar{P} \times \hat{N}) \quad (2)$$

From Newtonian impact theory:

$$C_D = 2 \cos^2 \theta = 2 (\hat{V}_T \cdot \hat{N})^2 \quad (3)$$

Where,

$$\hat{V}_T = \frac{\bar{V}_\infty - \bar{\omega} \times \bar{P}}{V_T}$$

For hypersonic velocities, the following approximation may be made:

$$\hat{V}_T \approx \frac{\bar{V}_\infty - \bar{\omega} \times \bar{P}}{V_\infty} \quad (4)$$

Substituting equations (4) and (3) into (2):

$$\Delta \bar{M} = 2 \left(\bar{V}_\infty \cdot \hat{N} - \frac{(\bar{\omega} \times \bar{P}) \cdot \hat{N}}{V_\infty} \right)^2 q_\infty \Delta A (\bar{P} \times \hat{N}) \quad (5)$$

Differentiating (5) with respect to a non-dimensional roll rate:

$$\frac{\partial \overline{\Delta M}}{\partial \left(\frac{\rho b}{2V_\infty} \right)} = \frac{4V_\infty^2 \Delta A (\bar{\rho} \times \hat{N})}{b} \left(2(\hat{V}_\infty \cdot \hat{N}) - \frac{(\bar{\omega} \times \bar{\rho}) \cdot \hat{N}}{V_\infty} \right) \frac{(-\hat{i} \times \bar{\rho}) \cdot \hat{N}}{V_\infty} \quad (6)$$

For hypersonic velocities:

$$|\hat{V}_\infty \cdot \hat{N}| \gg \left| \frac{(\bar{\omega} \times \bar{\rho}) \cdot \hat{N}}{V_\infty} \right|$$

Substituting equation (3) and using the above approximation, equation (6) reduces to:

$$\frac{\partial \overline{\Delta M}}{\partial \left(\frac{\rho b}{2V_\infty} \right)} = \frac{-8}{b^2} \Delta A (\bar{\rho} \times \hat{N}) \cos \theta (\hat{i} \times \bar{\rho}) \cdot \hat{N} \quad (7)$$

When the two vector products are evaluated, resulting x-component is:

$$\frac{\partial L}{\partial \left(\frac{\rho b}{2V_\infty} \right)} = \frac{-8}{b^2} \Delta A (y_c n_z - z_c n_y)^2 \cos \theta \quad (8)$$

Non-dimensionalizing (8), the desired form is:

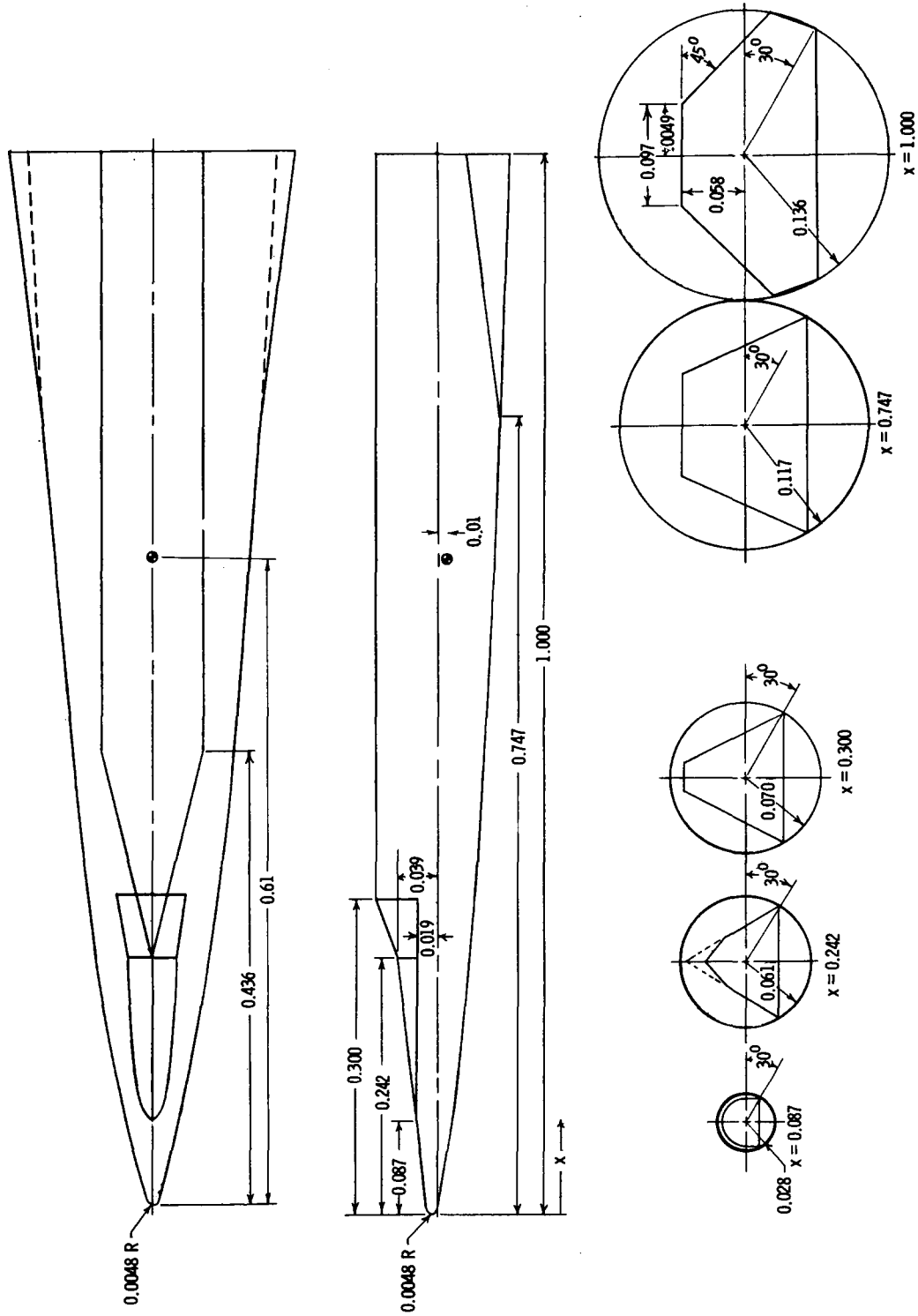
$$C_{lr} = \frac{-8}{b^2 S} (y_c n_z - z_c n_y)^2 \cos \theta \Delta A$$

In a similar manner the remaining dynamic stability derivatives may be evaluated, yielding:

$$C_{lr} = C_{rb} = \frac{-8}{b^2 S} (x_c n_y - y_c n_x) (y_c n_z - z_c n_y) \cos \theta \Delta A$$

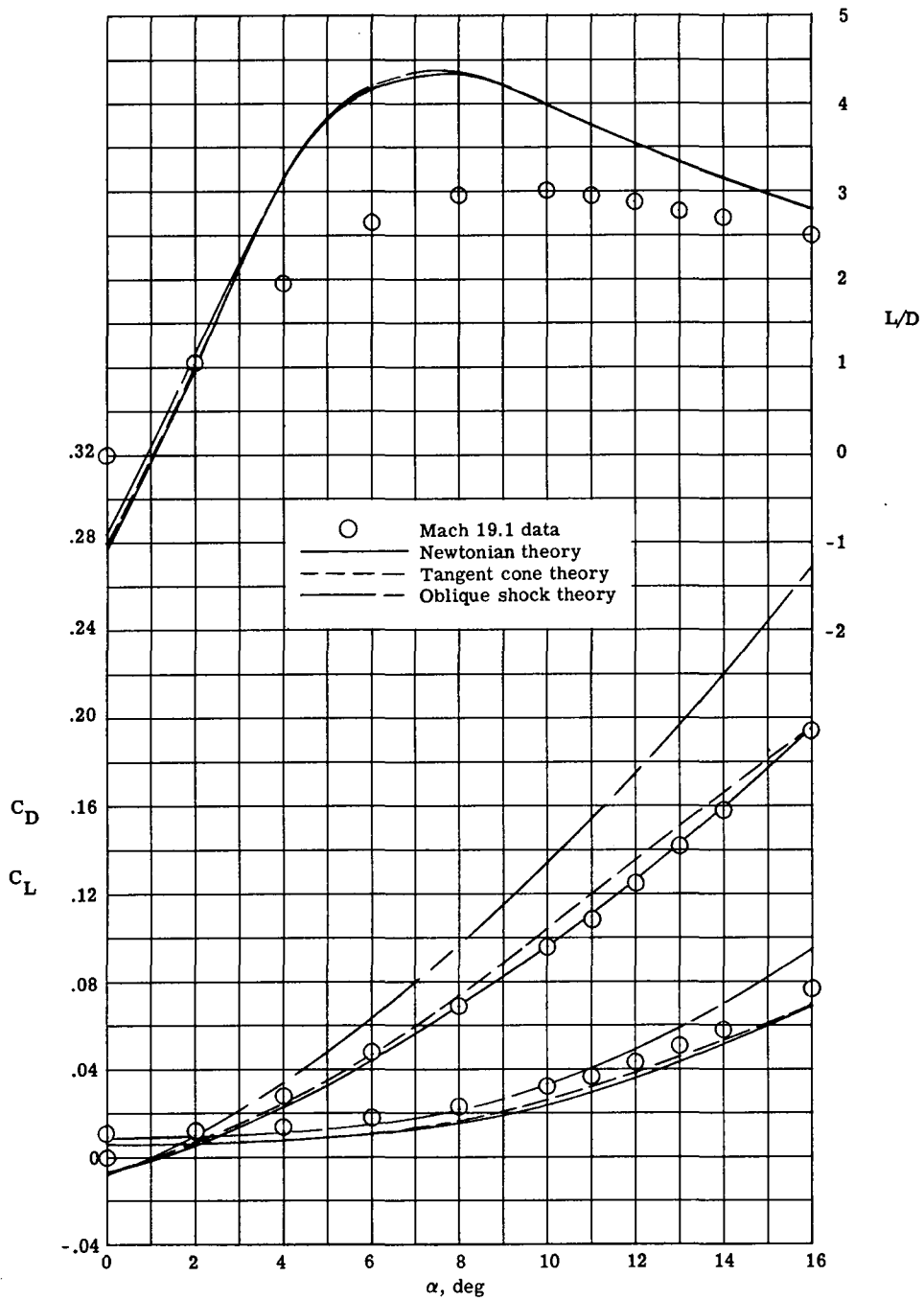
$$C_{nr} = \frac{-8}{b^2 S} (x_c n_y - y_c n_x)^2 \cos \theta \Delta A$$

$$C_{mq} = \frac{-8}{l^2 S} (z_c n_x - x_c n_z)^2 \cos \theta \Delta A$$



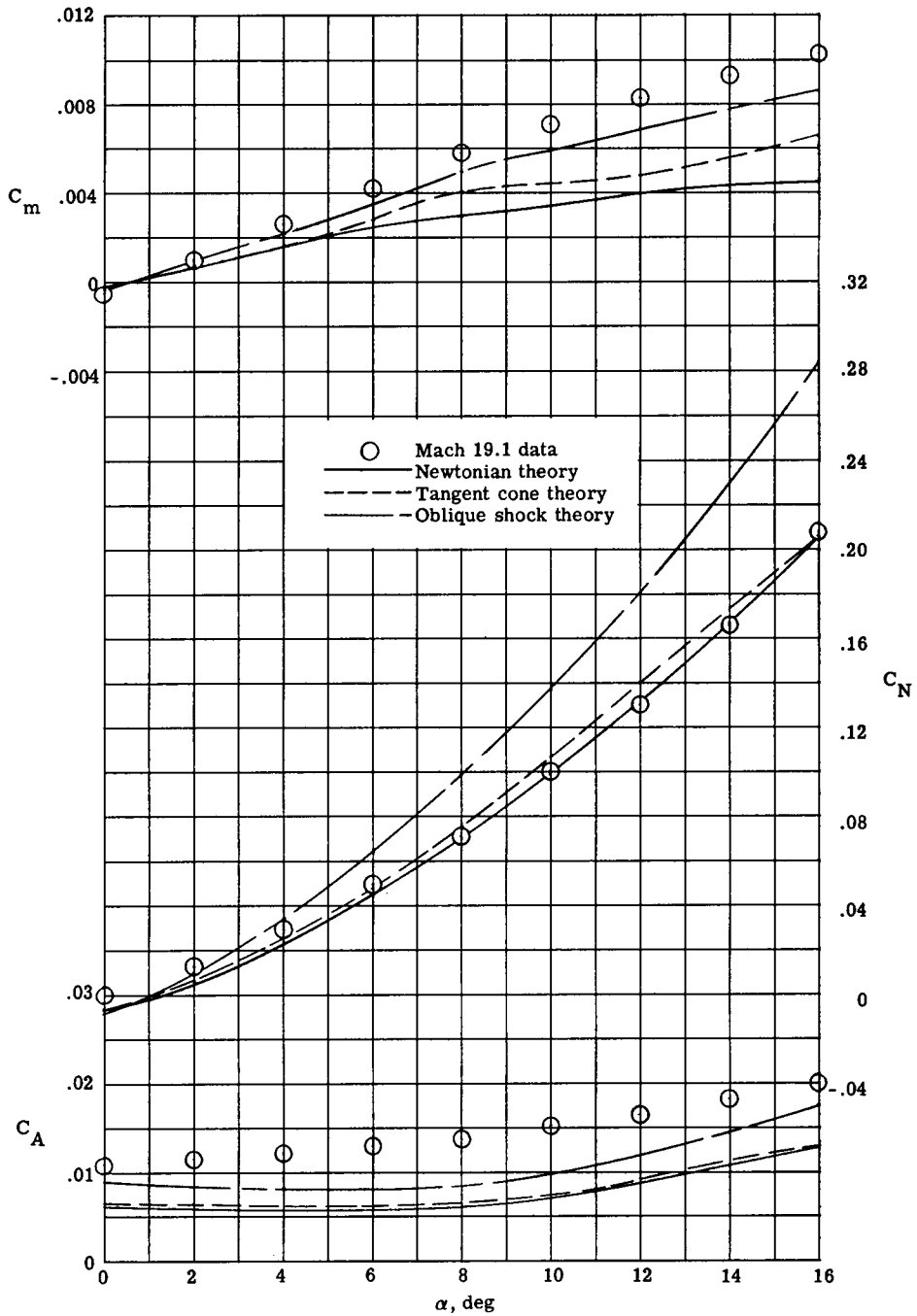
All lengths nondimensionalized by l

Figure 1.- Basic body definition.



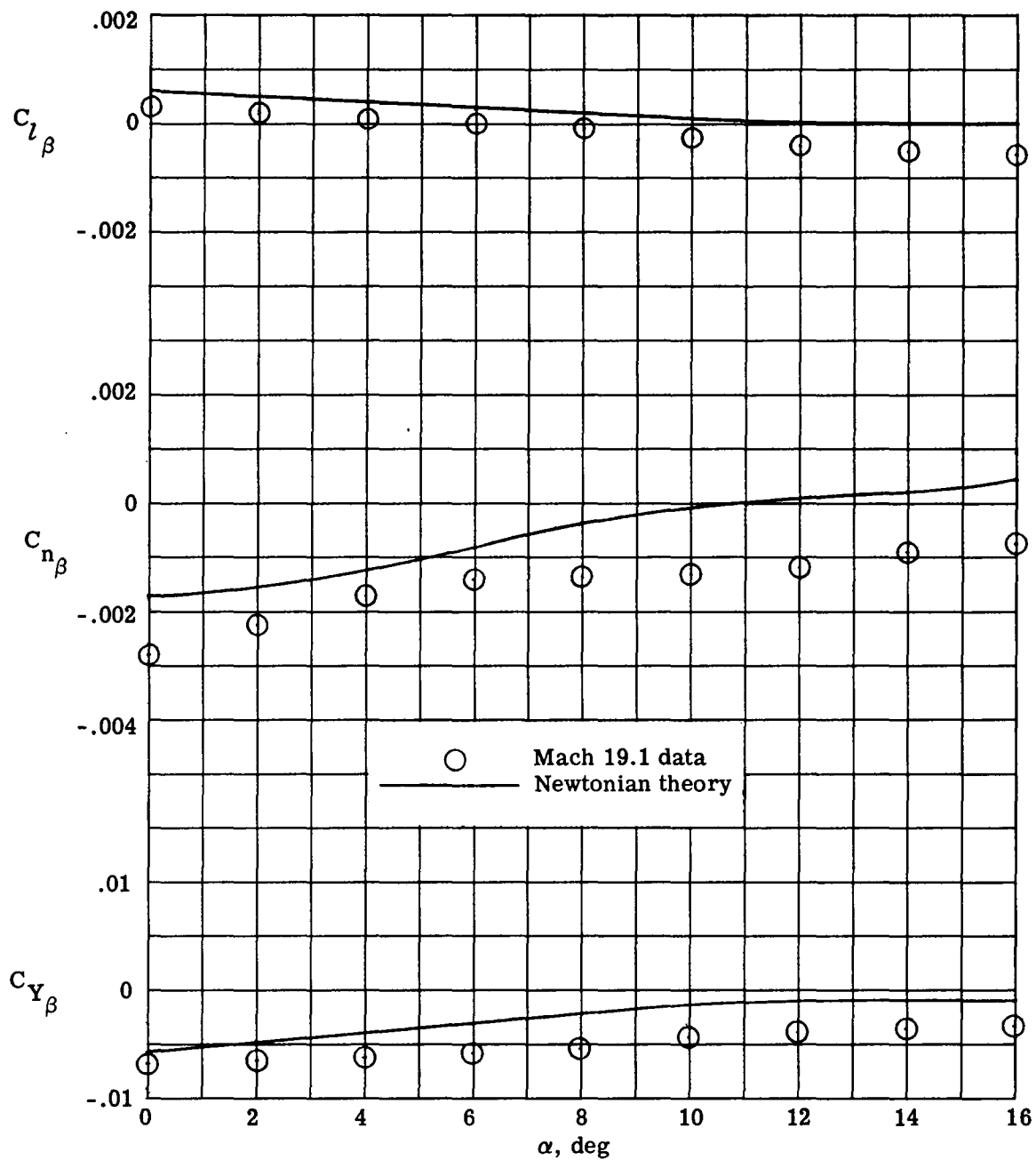
(a) Performance

Figure 2.- Comparison of basic body theoretical and experimental aerodynamic characteristics.



(b) Body axis.

Figure 2.- Continued.



(c) Lateral-directional static stability.

Figure 2.- Concluded.

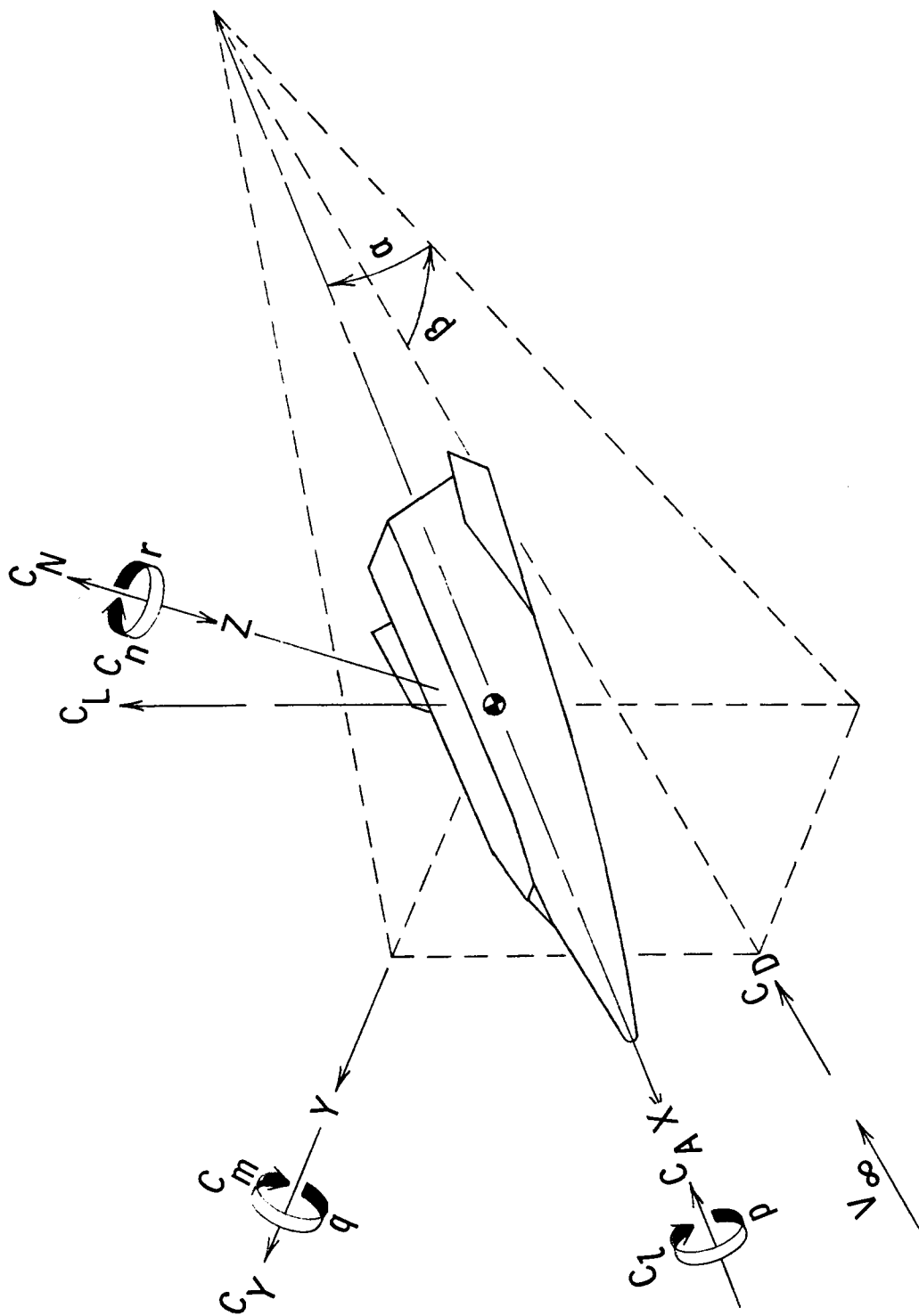
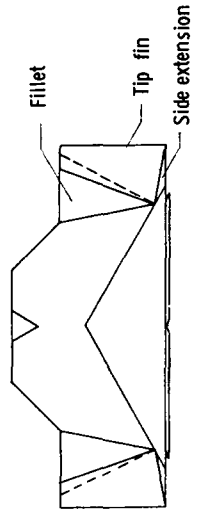
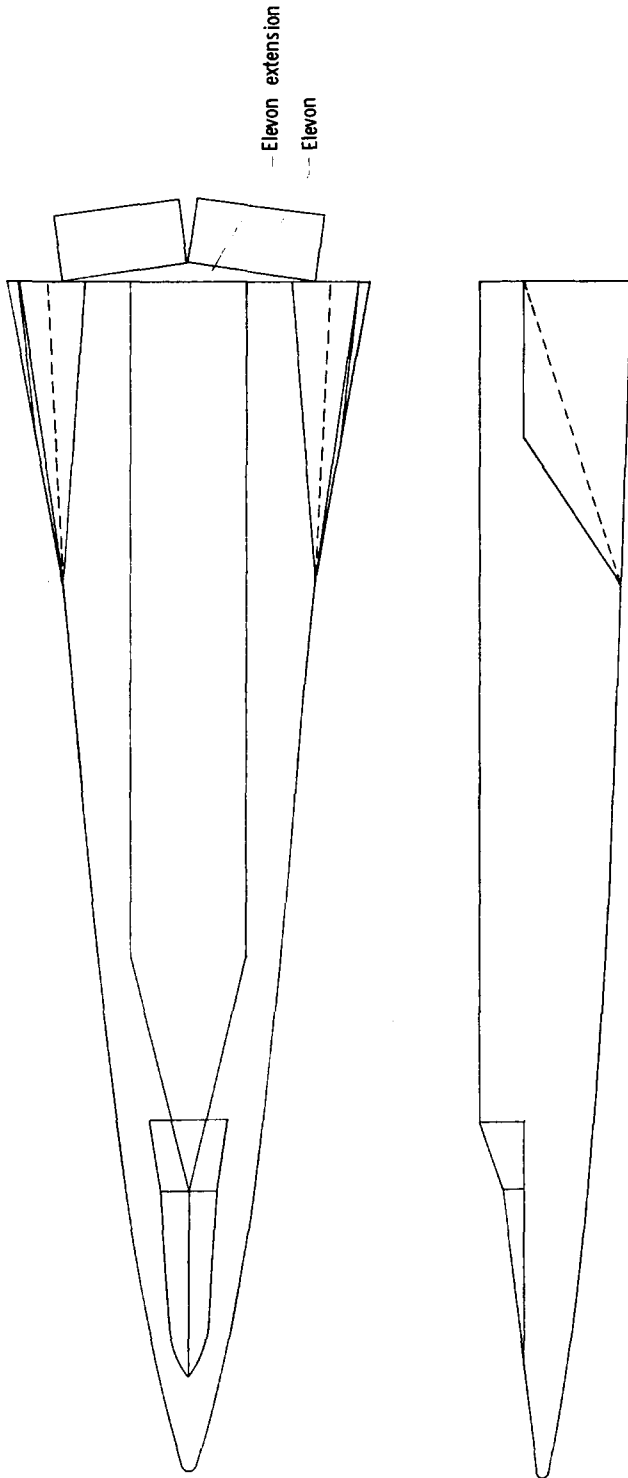


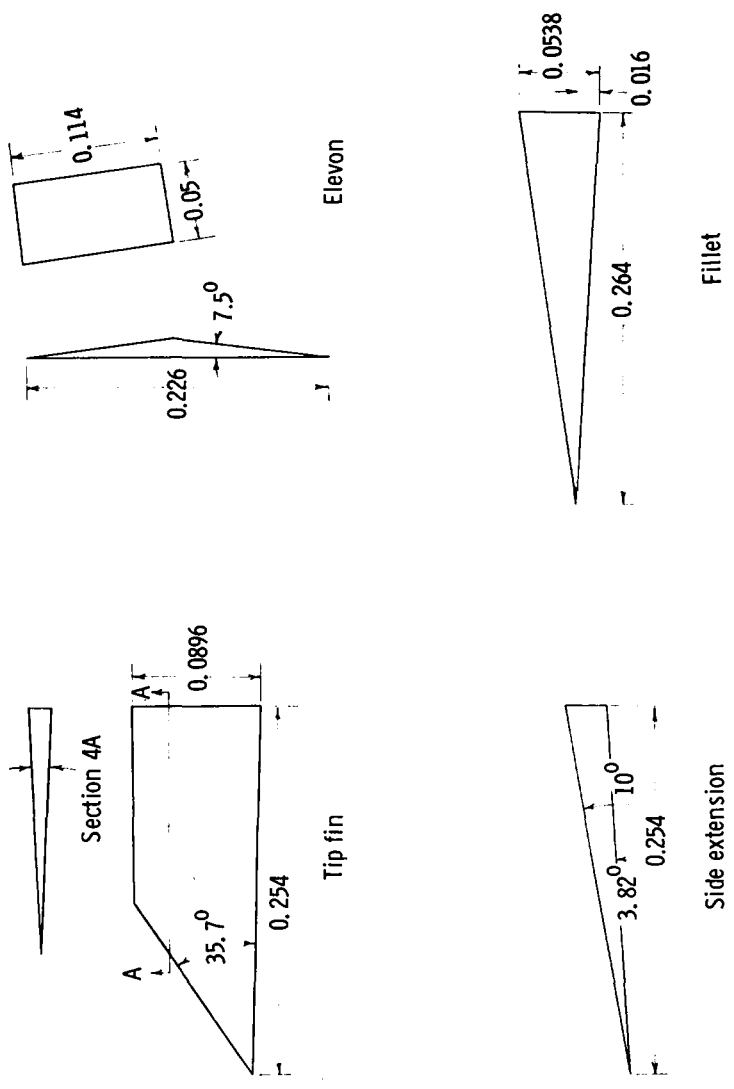
Figure 3.- Axis system.



Tip fin projected area (one fin) = $\frac{\text{Area}}{S} = 0.107$
 Fillet projected area = $\frac{\text{Area}}{S} = 0.063$
 Tip fin toe-in angle = 10°
 Tip fin roll-out angle = 0°

(a) Complete vehicle.

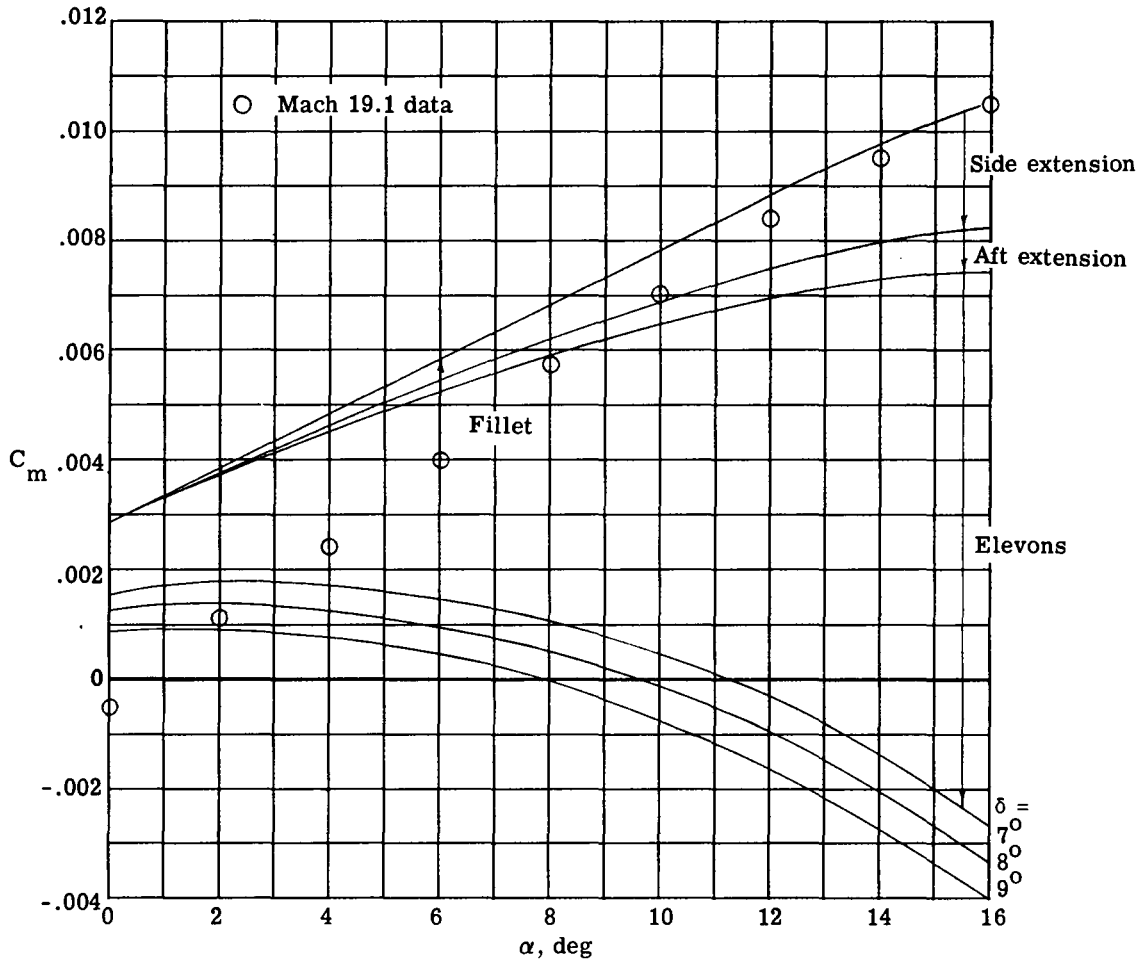
Figure 4.- Definition of stability and control devices.



	Area/S
Side extensions	0.0265
Aft extensions	.0106
Elevons	.0673

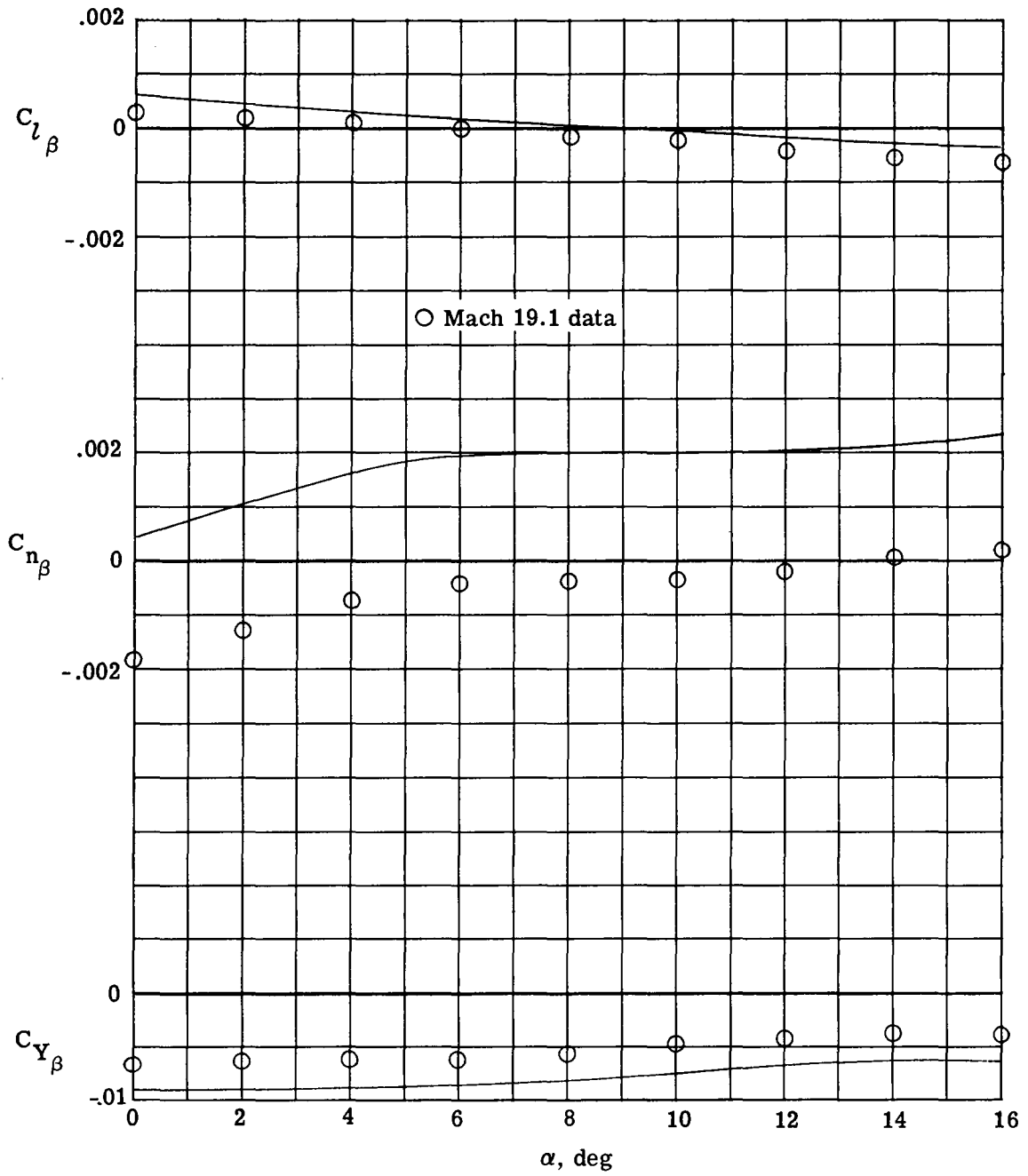
(b) Componets.

Figure 4.- Concluded.



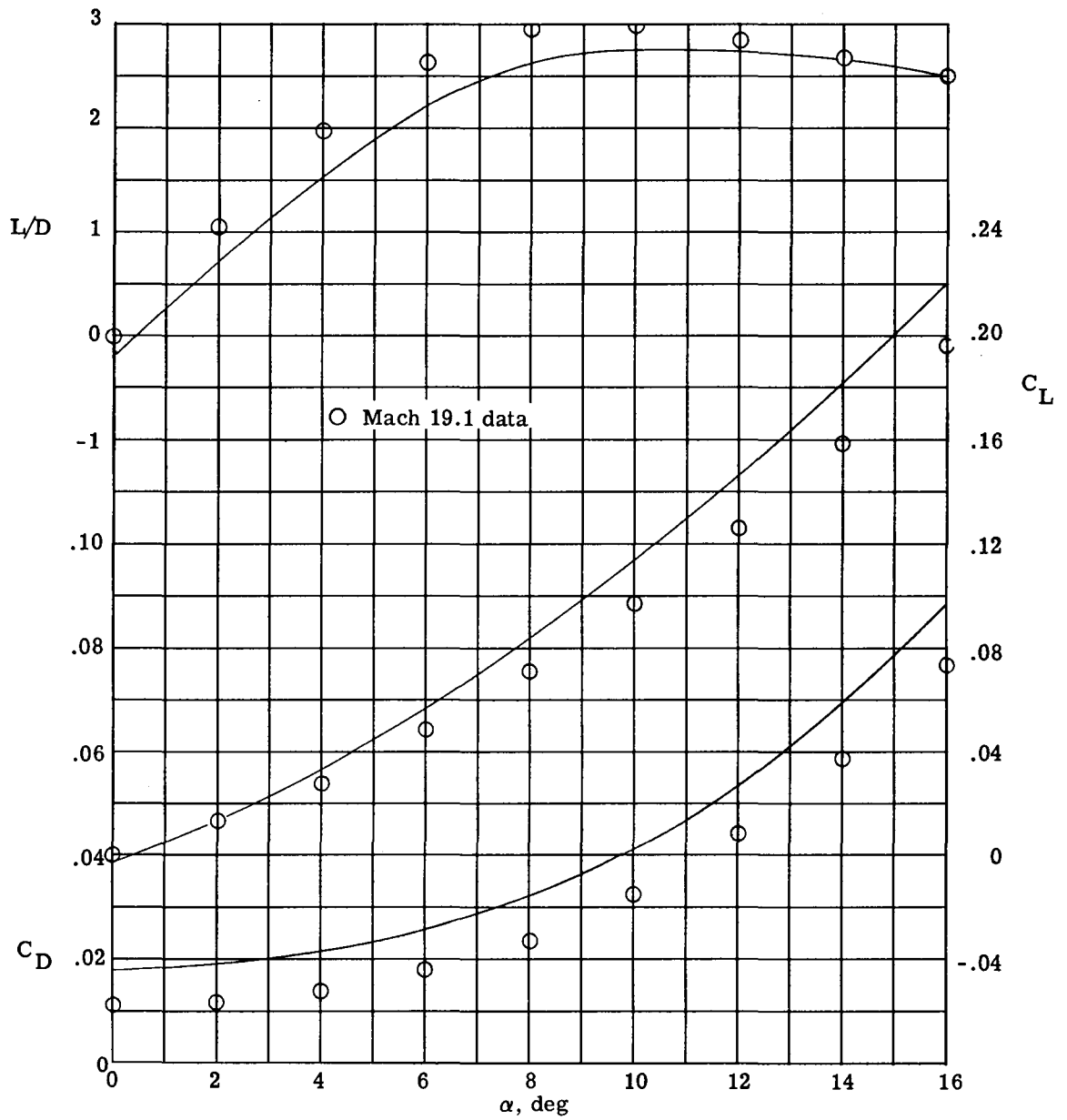
(a) Longitudinal stability.

Figure 5.- Vehicle trimmed aerodynamic characteristics.



(b) Lateral-directional stability.

Figure 5.- Continued.



(c) Performance.

Figure 5.- Concluded.

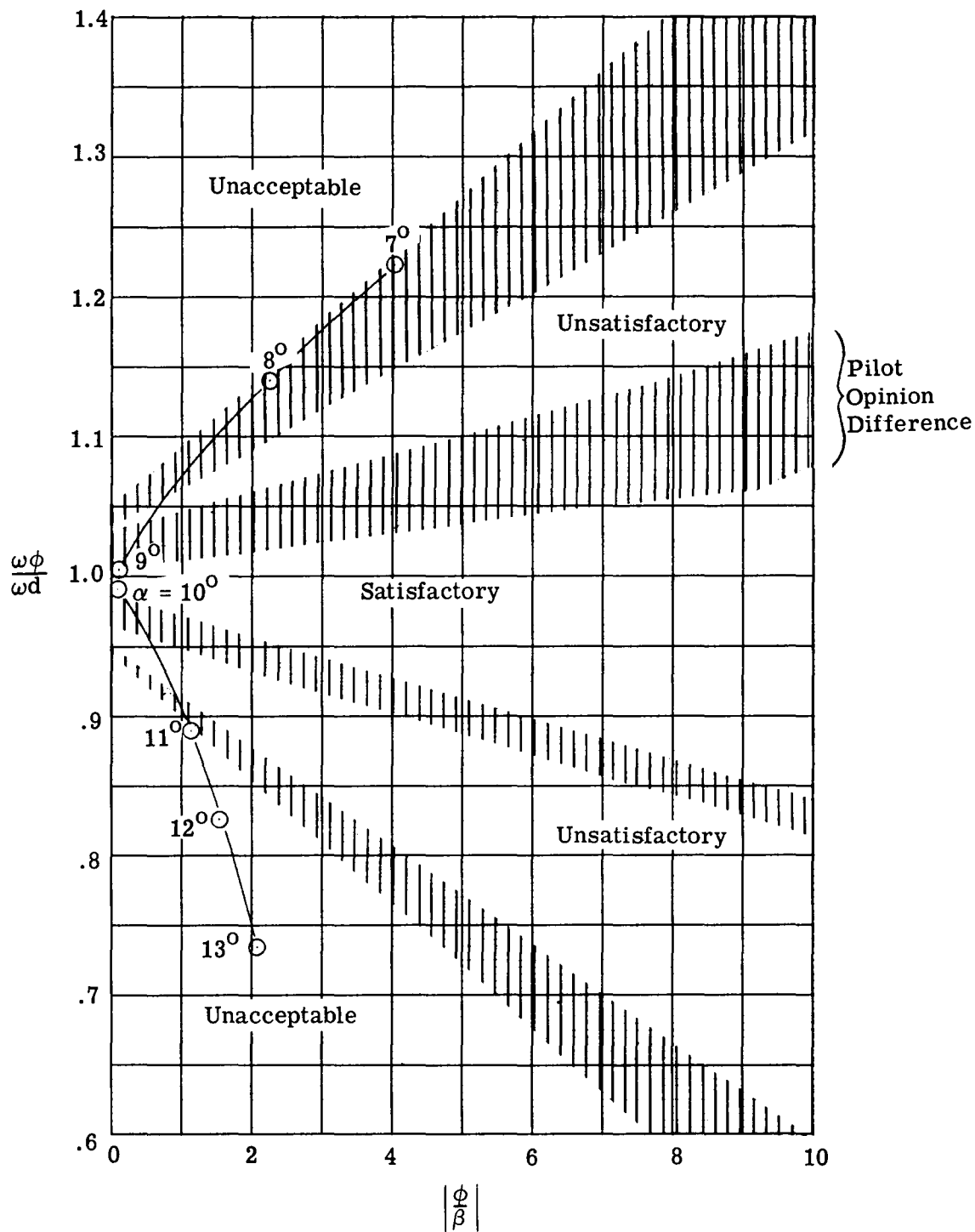


Figure 6.- Reentry vehicle handling qualities, reference 5.

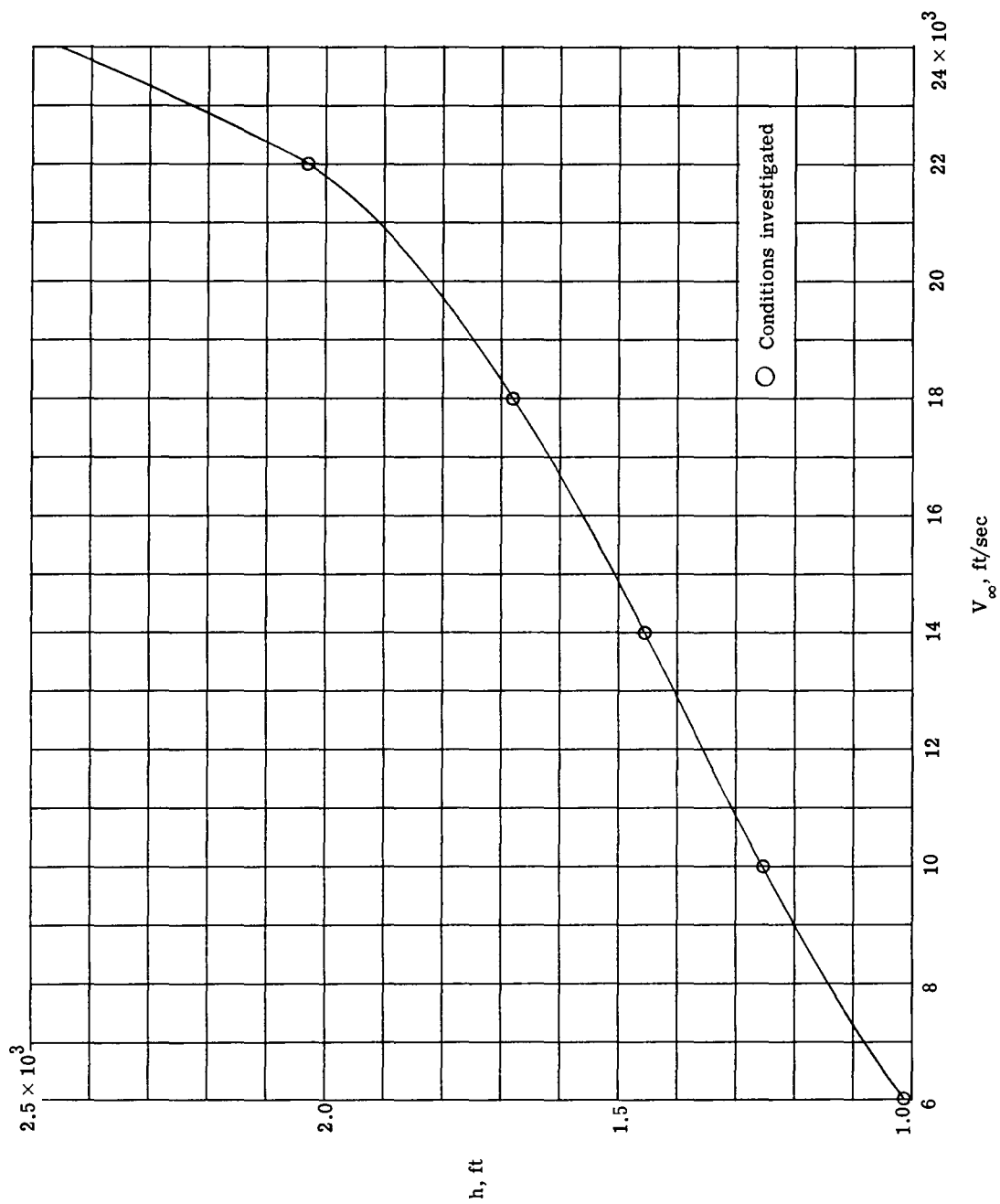


Figure 7.- Trajectory for maximum performance entry.

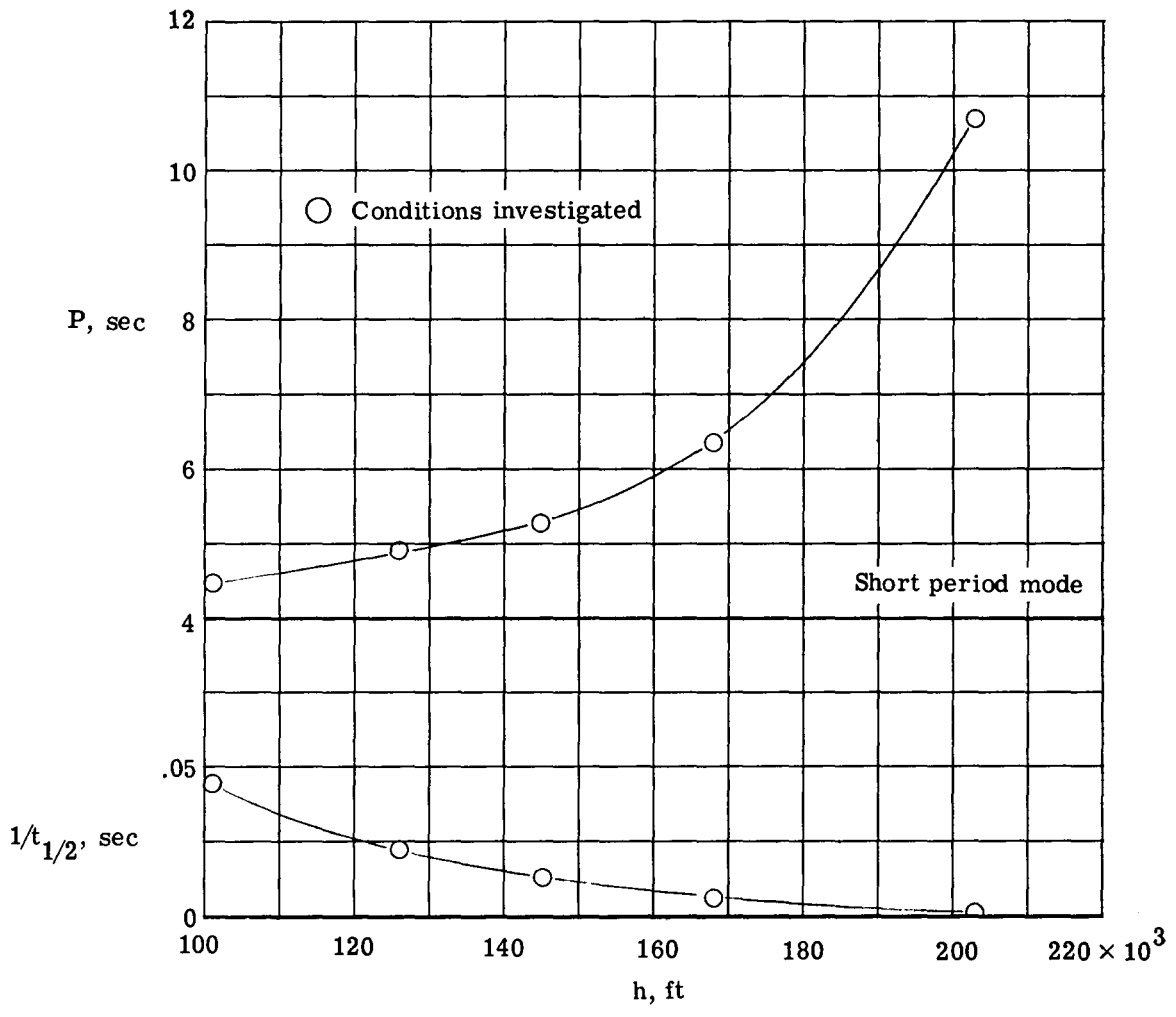


Figure 8.- Longitudinal transient characteristics.

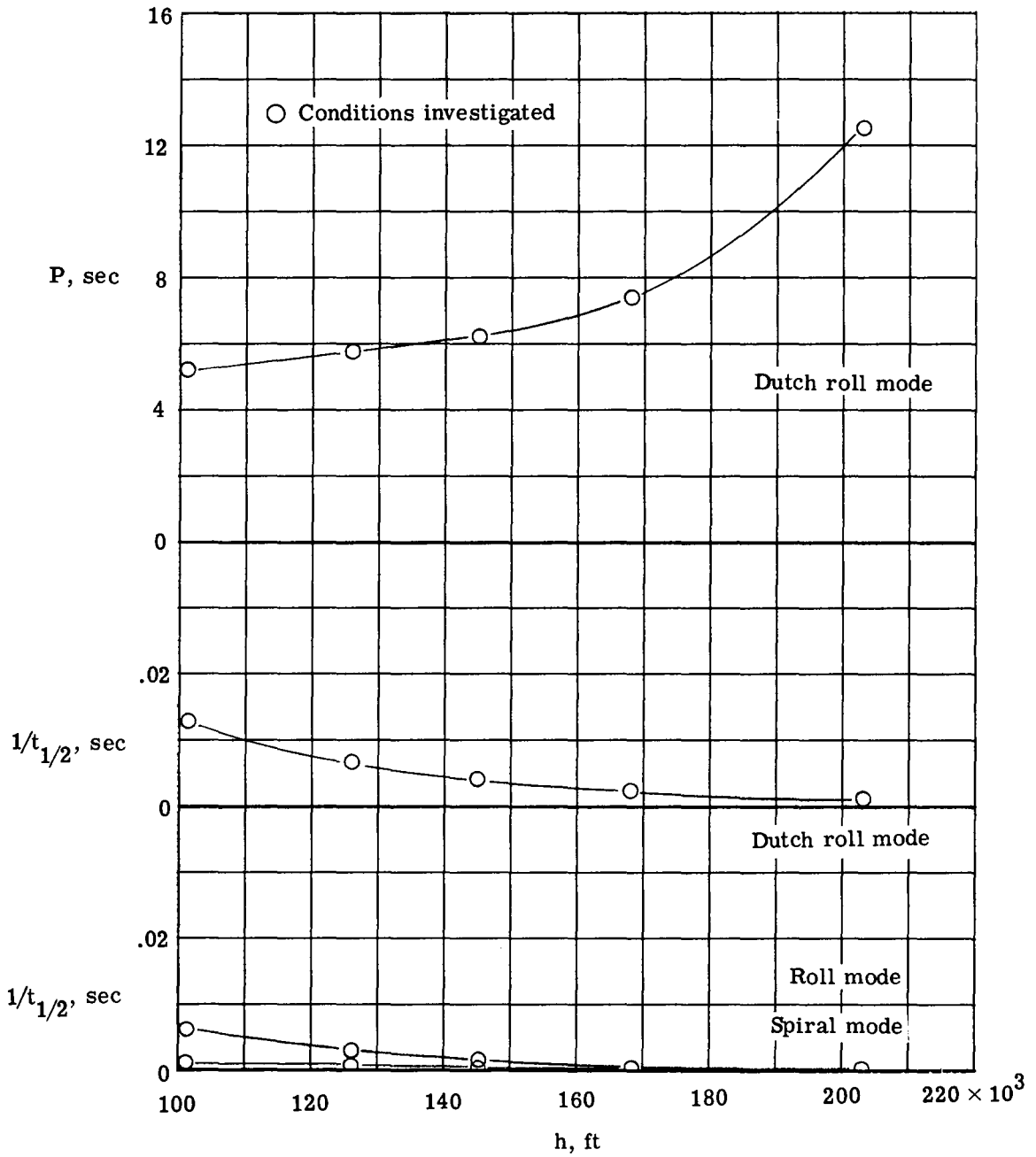


Figure 9.- Lateral-directional transient characteristics.

**The vita has been removed from
the scanned document**

AN ANALYSIS OF THE STATIC AND DYNAMIC
CHARACTERISTICS OF A DECOUPLED LANDING ENTRY VEHICLE

by

James Ernest Haile

ABSTRACT

A theoretical analysis of the static and dynamic characteristics of an entry vehicle utilizing the decoupled landing concept has been conducted. A hypersonic arbitrary-body aerodynamic computer program was used to determine the aerodynamics of the basic body. Three theories were used and compared with data obtained for a Mach number equal to nineteen. Several stabilizing devices were investigated to determine which were the most effective in providing static stability. To evaluate the lateral-directional handling qualities, a $\frac{\omega_\phi}{\omega_d}$ coupling parameter along with the parameter $\left| \frac{\phi}{\beta} \right|$ were derived to be applicable during hypersonic entry. Equations were also derived for determining the contribution of the stabilizing devices to the dynamic stability derivatives. In the evaluation of the vehicle dynamic characteristics linearized equations of motion for the longitudinal and lateral-directional modes were used at several points along a maximum performance trajectory. The parameters considered throughout the trajectory were the period and the time to damp to one-half amplitude.